Preprint
UCRL-JC-141229

Synthesis and Characterization of Porous Hydroxyapatite and Hydroxyapatite Coatings

T. G. Nieh, B. W. Choi, A. F. Jankowski

This article was submitted to
2001 Minerals, Metals, & Materials Society Annual Meeting & Exhibition, New Orleans, LA, February 11-15, 2001

October 25, 2000

U.S. Department of Energy
Lawrence Livermore National Laboratory

This work was performed under the auspices of the United States Department of Energy by the University of California, Lawrence Livermore National Laboratory under contract No. W-7405-Eng-48.

SYNTHESIS AND CHARACTERIZATION OF POROUS HYDROXYAPATITE AND HYDROXYAPATITE COATINGS

T. G. Nieh*, B.W. Choi, and A.F. Jankowski

* Lawrence Livermore Lab., L–350, P.O. Box. 808, Livermore, CA 94551, USA

Abstract

A technique is developed to construct bulk hydroxyapatite (HAp) with different cellular structures. The technique involves the initial synthesis of nanocrystalline hydroxyapatite powder from an aqueous solution using water–soluble compounds and then followed by spray drying into agglomerated granules. The granules were further cold pressed and sintered into bulks at elevated temperatures. The sintering behavior of the HAp granules was characterized and compared with those previously reported. Resulting from the fact that the starting HAp powders were extremely fine, a relatively low activation energy for sintering was obtained. In the present study, both porous and dense structures were produced by varying powder morphology and sintering parameters. Porous structures consisting of open cells were constructed. Sintered structures were characterized using scanning electron microscopy and x–ray tomography. In the present paper, hydroxyapatite coatings produced by magnetron sputtering on silicon and titanium substrates will also be presented. The mechanical properties of the coatings were measured using nanoindentation techniques and microstructures examined using transmission electron microscopy.

1. Introduction

Calcium phosphate apatite is one of the most viable implant materials because of its excellent biocompatibility [1]. In fact, cortical bone is composed of approximately 60–70 wt% mineral and 30 wt% organic constituents [2, 3]. The major subphase of the mineral consists of submicroscopic crystals of an apatite of calcium and phosphate, resembling hydroxyapatite (HAp) in its crystal structure [$Ca_{10}(PO_4)_6(OH)_2$]. The HAp is nanocrystalline with grains in the size of 10–50 nm. These nanometer–sized grains are hierarchically assembled into connective hard tissue, i.e. bone–skeleton [4].

Two types of HAp are employed as implant material: bulk monolithics and coatings. In the case of bulk, there is a growing interest in developing porous HAp structures [5, 6]. This development results from the fact that human bones, in particular cancellous bones, are primarily macroporous [7]. In the case of bone grafting, it is also known that bone defect regenerates more predictably if a stromal substitute is implanted to provide a framework for

organization of the osteons. The development of HAp with a proper morphological structure compatible with the osteons and their vascular interconnections is, therefore, of great interest. Commercial porous HAp is processed by the thermo-conversion of calcium carbonate (coral) to calcium phosphate [6]. After conversion, the coral still retains its original pore morphology (~100-200μm pore size). However, it is highly desirable that HAp powder can be used as the starting material to artificially build porous HAp. To be able to prepare porous HAp with a controlled morphology, it is necessary to understand first the sintering kinetics of HAp. Several studies have been carried out on the sintering behavior of HAp powder with different sizes and morphologies [8-11]. In the first part of the present paper, sintering behavior of nanocrystalline HAp is presented.

In the case of coatings, HAp is applied to metallic implants (Ti- or Co-based alloys) to improve biocompatibility and to minimize chemical dissolution of metals by body fluid. Plasma spray technique has been widely used as a result of the fast deposition rate and economic benefit. However, coating adhesion is often poor and chemical composition of the HAp coating is not stoichiometric. As a result of a highly non-equilibrium process. HAp coatings usually contain undesirable CaO, tri- and tetra-calcium phosphates, and amorphous calcium phosphate [12]. To improve interfacial adhesion, magnetron sputtering [13, 14] and ion-beam dynamic mixing [15] methods have been prepared. However, the mechanical properties of the coating as well as the interface properties have not been carefully investigated. Thus, in the second part of this paper, HAp coatings will be produced by magnetron sputtering on Ti and Si substrates. The mechanical and interface properties of the coatings will be discussed.

2. Material and Experimental Procedure

An aqueous solution was first prepared by mixing calcium and phosphorous in a 5:3 ratio. Fine HAp precipitates were obtained from a solution whose alkalinity was adjusted to a pH value of 11 by adding ammonia solution (NH_4OH). These precipitates were subsequently rinsed several times to remove residual NH_4OH. These precipitates were further mixed with distilled water to result in a suspension. A spray dry process was, then, used to produce HAp powders with various particle sizes and morphologies. (The spray drying process has been described previously [16].) The inlet and outlet temperatures of the spray dryer were 100 and 200°C, respectively. The spray dried powders are essentially agglomerates, as revealed by transmission and scanning electron microscopy (TEM and SEM).

The sprayed powders were initially cold pressed into green bodies at a uniaxial pressure of 187 MPa. The green bodies were, then, sintered for 4 hours in air at temperatures varying from 700 to 1300°C. The density of sintered samples, ρ, was not measured using the conventional liquid immersion technique because of its open-pore structure. Rather, it was obtained by measuring the weight and physical dimension (volume) of the sintered samples. (The theoretical density of HAp is 3.219 g/cm^3 [4].) The microstructure of all sintered samples was examined using scanning and transmission electron microscopy (SEM and TEM). Structural characterization was performed by using x–ray analysis (XRD). The microhardness of the sintered samples was measured using a Vickers Microhardness Tester.

The coatings of this study are prepared by sputter deposition using planar magnetrons operated in the dc and RF mode. The high vacuum chamber is cryogenically pumped to a base pressure of 6 μPa. Each planar magnetron has a 63 mm diameter and is horizontally positioned at a source-to-substrate separation of 102 mm. The target materials are 99.94% pure titanium and hydroxyapatite. The substrate wafers are polished, single crystal (111) silicon and wafers that are sputter coated with a 1 μm thick layer of titanium (denoted as Ti/Si substrate). The substrate table is held at room temperature. The hydroxyapatite coatings are deposited operating the magnetrons in the RF at a forward power of 75 Watts using a working gas pressure of 1.3 Pa at a flow rate of 40 cc min^{-1}. Two film thicknesses were produced. In

the case of 0.65 μm-thick hydroxyapatite coating, it was produced using a working gas of pure Ar whereas in the case of 0.35 μm-thick coating, a working gas mixture of Ar-3%O_2 was used.

The microstructure of the 0.65μm HAp/Ti/Si film was examined using transmission electron microscopy. Nanoindentation tests were carried on the coated samples with a Nano Indenter XP. Hardness and elastic modulus were measured using the continuous stiffness option, which yields elastic modulus and hardness as a function of indentation depth. A Berkovich indenter was used in the experiments. A quartz sample was used as a standard for the initial calibration.

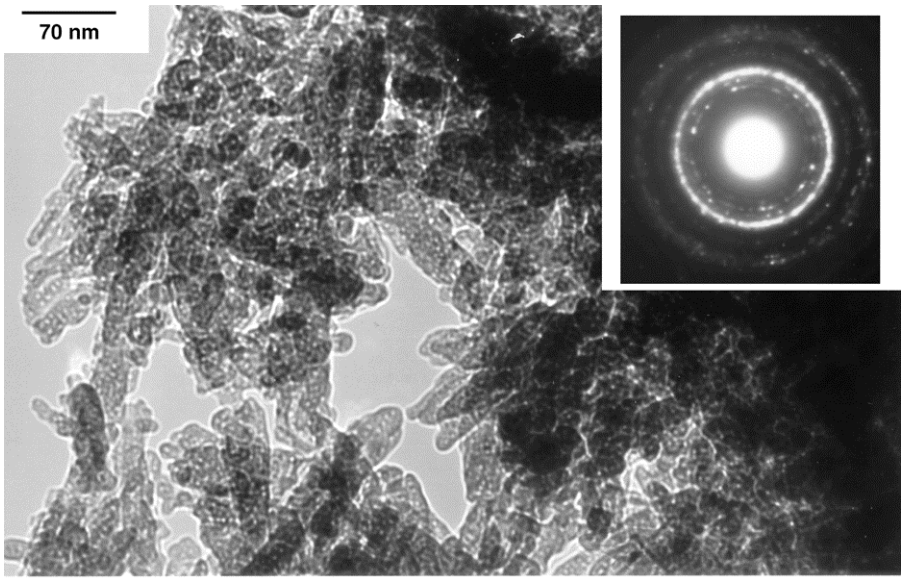

Fig. 1 TEM bright field image showing the needle-like HAp nanocrystalline crystals.

3. Results

3.1 Sintering

The chemical precipitation method used to synthesize HAp particles is described by the following chemical reaction:

$$10Ca(OH)_2 + 6H_3PO_4 \xrightarrow[\text{Room temp.}]{NH_4OH} Ca_{10}(PO4)_6(OH)_2 + 18H_2O \qquad (2)$$

As shown in Fig. 1, the precipitated HAp has a needle–shape morphology (~ 10–20 nm in width and 60–90 nm in length), similar to that of the apatite particles existing in natural bones [4]. X–ray diffraction pattern indicates that these HAp particles are polycrystalline with a preferred [211] orientation. These needle–shape nanocrystalline particles were further suspended and sprayed to yield large–sized particles [16]. The sprayed powders are essentially spherical with a mean size of approximately 1.8 μm (the maximum size is about 5 μm).

The density of a pre–sintered solid (i.e. green body) is 1.42±0.15 g/cm^3 (approximately 44% of the theoretical density). Experimental results obtained from sintering experiments are listed in Table 1. Each datum point was from a minimum of 8 readings. As indicated in the table, at the lowest sintering temperature (700°C), the density (44 %) is similar to that of the green body. The density is noted to increase with sintering temperature and reaches a nearly fully dense value (99%) at 1300°C. The grain structure of the 99%–dense sample is shown in Fig. 2. This image reveals equilibrated, hexagonal–shaped grains with sharp apexes with a

mean grain size of about 4 μm. X–ray diffraction analysis indicates that the sample contains also a slight amount (less than 1%) of tri-calcium phosphate (TCP). This is, somewhat, expected since apatite is essentially a line compound, which is technically difficult to obtain in a pure form.

The fracture surfaces of samples sintered at different temperatures are shown in Fig. 3. At the lowest sintering temperature (700°C), no sintering takes place and pores are less than 0.5 μm. At 900°C, sintering begins – necks form between particles and large pores grow at the expense of small pores. At 1000°C, a skeletal structure begins to develop – the struts in the skeleton appear to be continuous and interconnected pores are revealed. The pore sizes are about 1–2 μm. At yet a higher temperature of 1100°C, significant densification occurs. Finally, at the highest sintering temperature of 1300°C, the sample is practically fully dense and only a few pores are observed.

Table 1 Physical properties of HAp sintered at different temperatures

Temperature, °C	Relative density, *D*	Shrinkage, *S*	Microhardness, H_V
1300	99%	1.25	483
1200	88%	1.0	—
1180	84.5%	0.92	—
1100	84%	0.9	303
1000	71%	0.61	263
900	64%	0.45	208
700	44%	0	—
Green body	44%	—	—

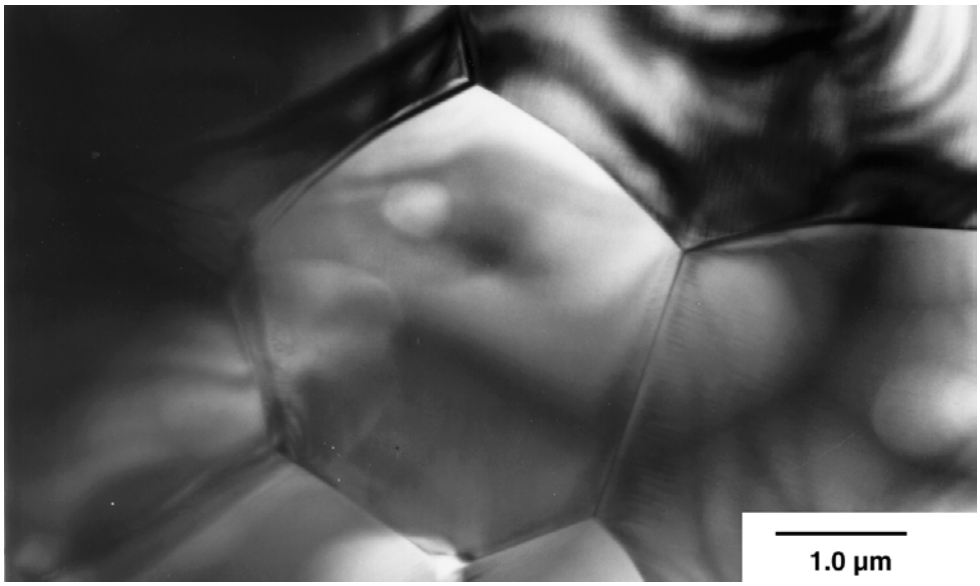

Fig. 2 TEM micrograph taken from the 99%–dense sample, showing a single-phase structure with a grain size of about 4 μm.

It is readily to observe in Table 1 that the microhardness value, ranging from 208 to 483 MPa, also increases with sintering temperature. In the present study, the microhardness of a de–mineralized human tooth (i.e. enamel) was also measured to be 325 MPa, which is softer than that of fully dense HAp (483 MPa). Nonetheless, the microhardness of enamel is within the data range for sintered HAp obtained in the present study. The microhardness of a sintered HAp sample is closely related to its density, specifically, the higher the density the harder is the sample, as shown in Fig. 4. The microhardness can be expressed with the relative density, D, in a simple mathematical form:

$$H_v \text{ (MPa)} = 7.5 \text{ D (\%)} - 279 \qquad (2)$$

This equation can be conveniently used to estimate the density of a sintered HAp sample.

The relative density of HAp samples as a function of the sintering temperature is plotted in Fig. 5. Within the temperature range, density increases monotonically with sintering temperature. Data from some of the previous studies [8, 10] are also included in the figure for comparison. The present data are noted to be slightly higher than those reported previously [8, 10], probably resulted from the fact that the starting HAp powders used in the present study are

ultrafine (nanocrystalline). As a result of being ultrafine, there is an exceedingly large amount of surface energy aid to the thermodynamic driving force for sintering.

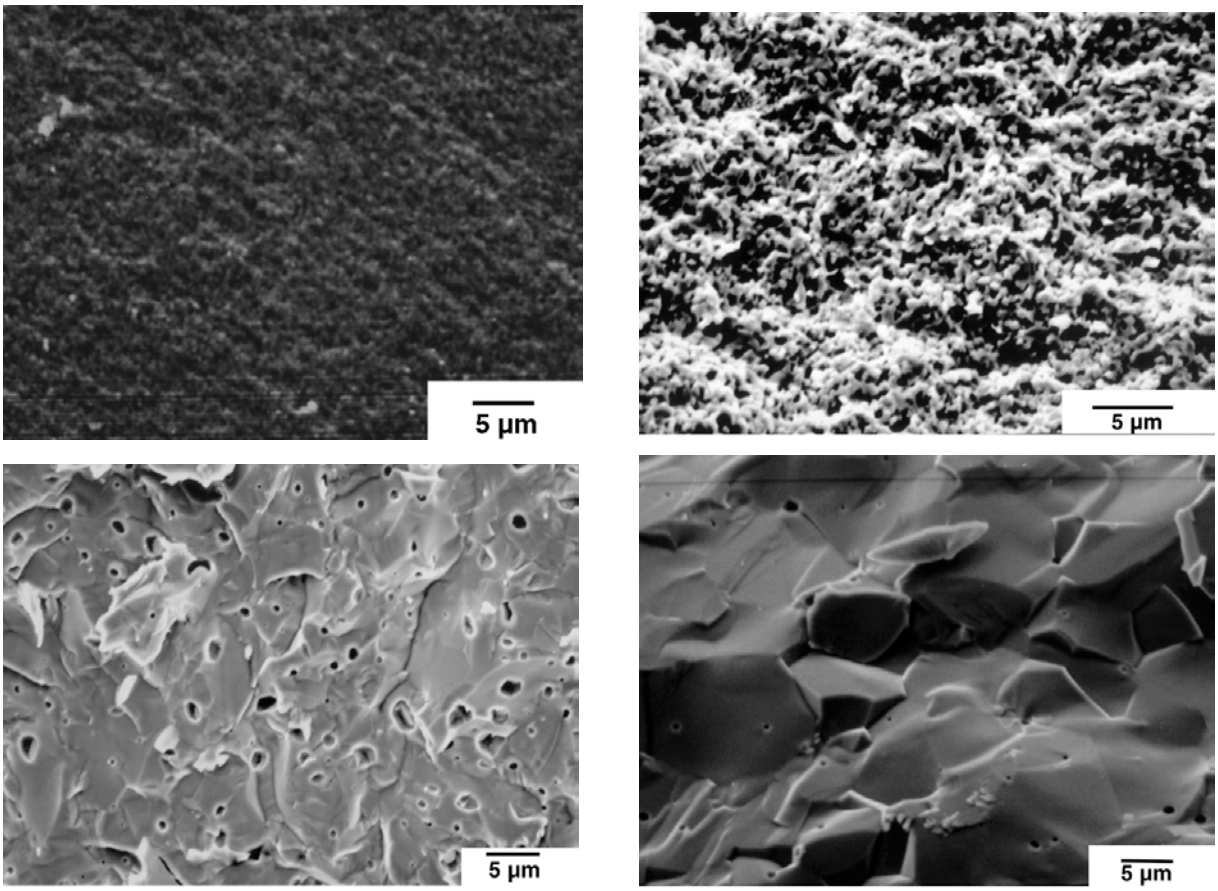

Fig. 3 Fracture surface appearance of various sintered samples. (upper left) 700°C, (upper right)-900°C, (lower left)–1100°C, (lower right)–1300°C.

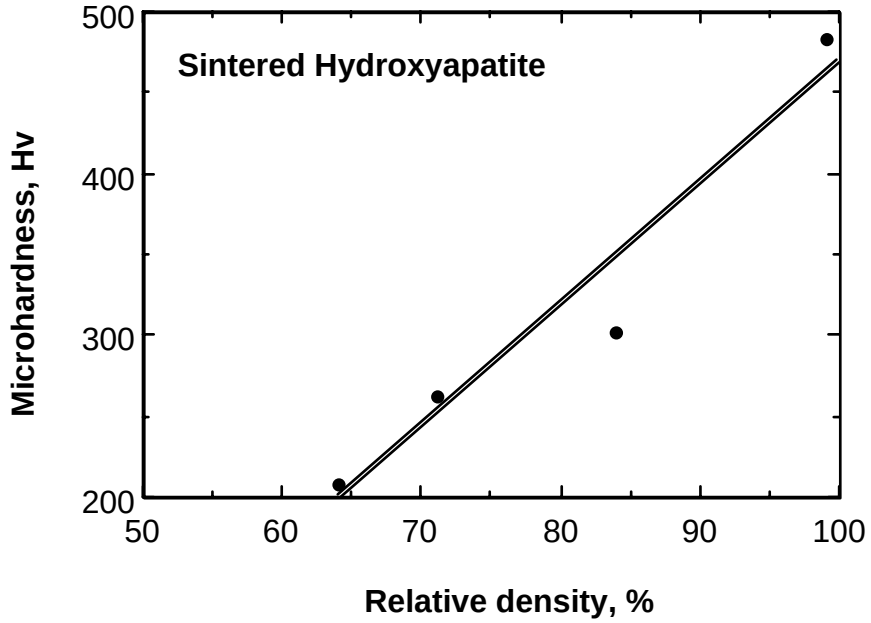

Fig. 4 Microhardness as a function of density for sintered hydroxyapatite.

Densification during sintering can be described by:

$$S = 1 - \frac{D_g}{D} \tag{3}$$

where S is the volume shrinkage, D and D_g, are the sintered and green densities, respectively.

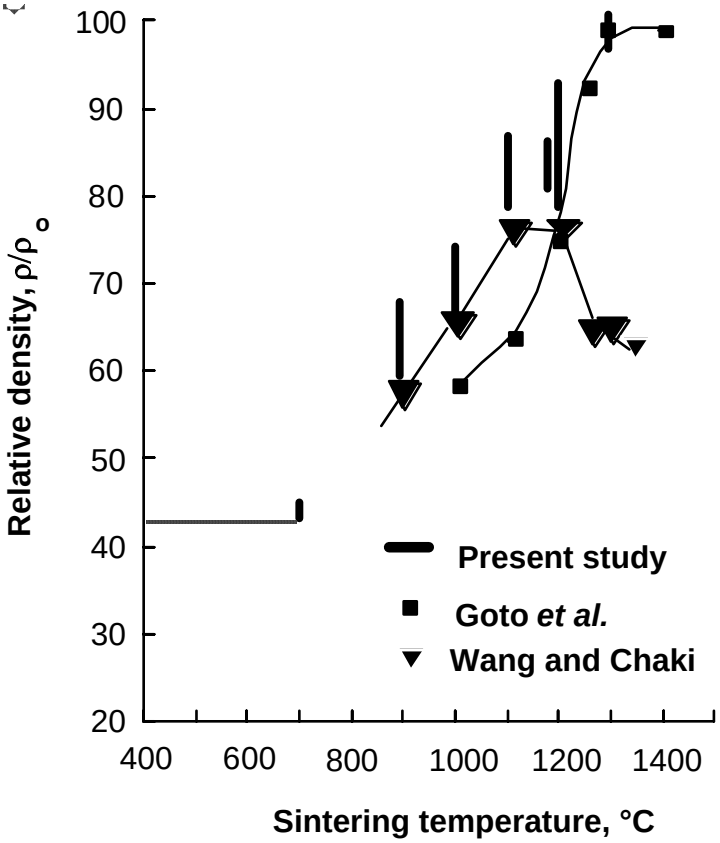

Fig. 5 Relative density of sintered HAp as a function of sintering temperature.

The shrinkage of a non–transforming solid, assuming an isothermal process, is

$$S \propto r^{-m} \tag{4}$$

where r is the particle radius, and m = 6/5 [17]. It is readily seen from Equation (4) that S increases rapidly with decreasing particle size. Thus, the accelerated sintering obtained in the present study is attributable to the nanometer-sized powder used.

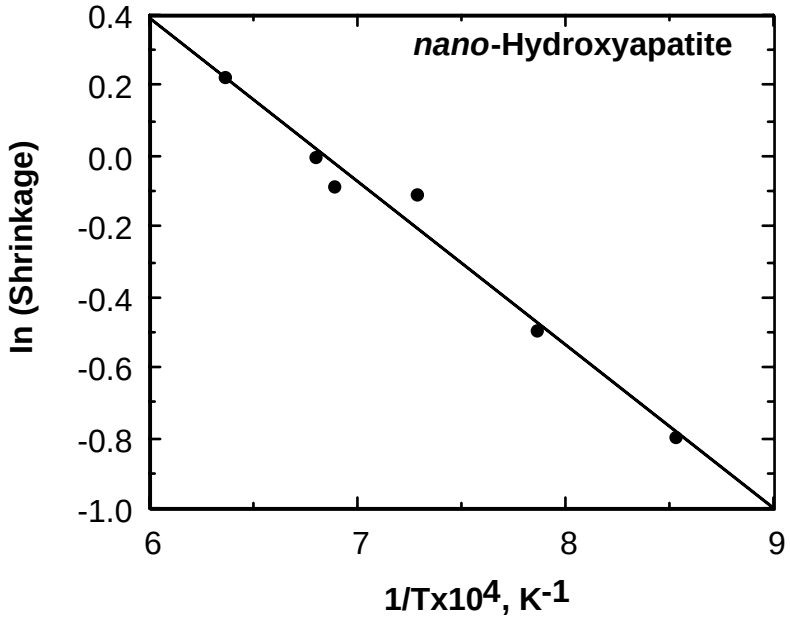

Fig. 6 Logarithm of shrinkage plotted as a function of the inverse of temperature for sintered nanocrystalline HAp.

According to Equation (3), the activation energy for sintering, *Q*, can be obtained from the Arrhenius plot (i.e. the logarithm of S vs the inverse of absolute temperature) shown in Fig. 6. It is calculated to be 96 kJ/mol, which is noted to be relatively low compared to those reported by Wang *et al.* (196 kJ/mol) [10], Jarco *et al.* (234 kJ/mol) [18], Kijima and Tsutsumi (238 kJ/mol) [19], de With *et al.* (142 kJ/mol) [11], and Goto *et al.* (161 kJ/mol) [8].

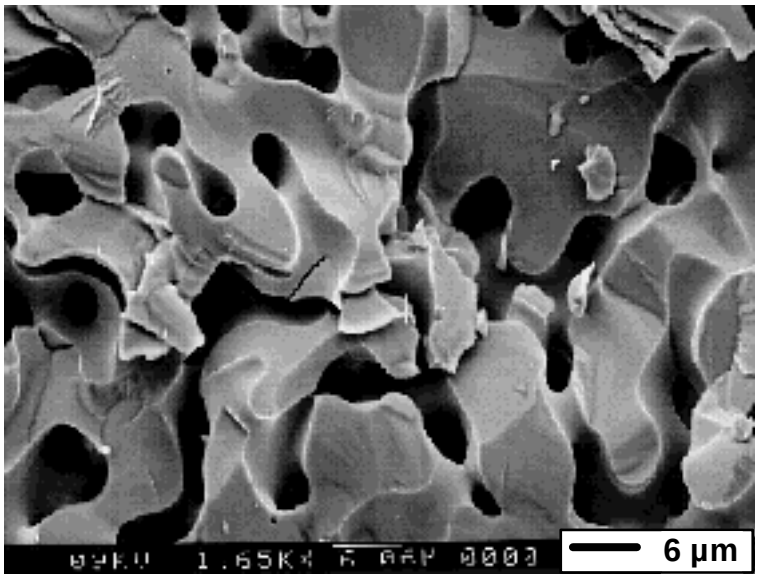

Fig. 7 A composite sample sintered at 1100°C for 4 hours with a density value of 51%. The micrograph reveals uniformly distributed pores of about 5 µm in size.

3.2 Cellular structure

Hulbert and Young [20] noted that in order to allow enough space to host the cellular and extracellular components of bone and the blood vessels, pores at least 100 µm in diameter are needed. These pores must be interconnected so as to enable the blood vessels to anastomose into each other and the implanted structure can still retain its mechanical integrity. Based on

the sintering results, initial attempts were made to fabricate porous HAp. Polymer beats with a diameter of 100 μm were added to HAp powder prior to sintering. The addition of polymer beats is to stimulate the formation of interconnected macropores in HAp skeleton during sintering. The density and morphology of the sintered composites depend upon sintering temperatures (1000°C–1300°C).

The SEM surface morphology of the composite sample sintered at 1100°C for 4 hours with a density value of 51% is shown in Fig. 7. The micrograph reveals that pores of about 6 μm in size which are uniformly distributed. To investigate the 3-dimensional interconnectivity, a x-tomographic technique was used [21]. Figures 8 shows the 3D scan of the cellular structure. The porosity content is estimated to be 47%, which is close to that measured from density measurement**.** It is obvious that the pore size is too small for practical application. The polymer beats apparently collapsed during the early stage of sintering and failed to serve their purpose. Assuming the solid-sphere model, the size of starting HAp powders, in principle, must be larger than the pore size. Thus, to produce pores of about 100-200μm, the starting powders must be greater than 100-200 μm.

3.3 Coating

A TEM microstructure of the as-deposited 0.65μm-thick HAp film is shown in Fig. 9. The film is fully dense and polycrystalline consisting of ultrafine grains with an average grain size of about 20 nm. They are randomly orientated, as revealed in an electron diffraction pattern (inset).

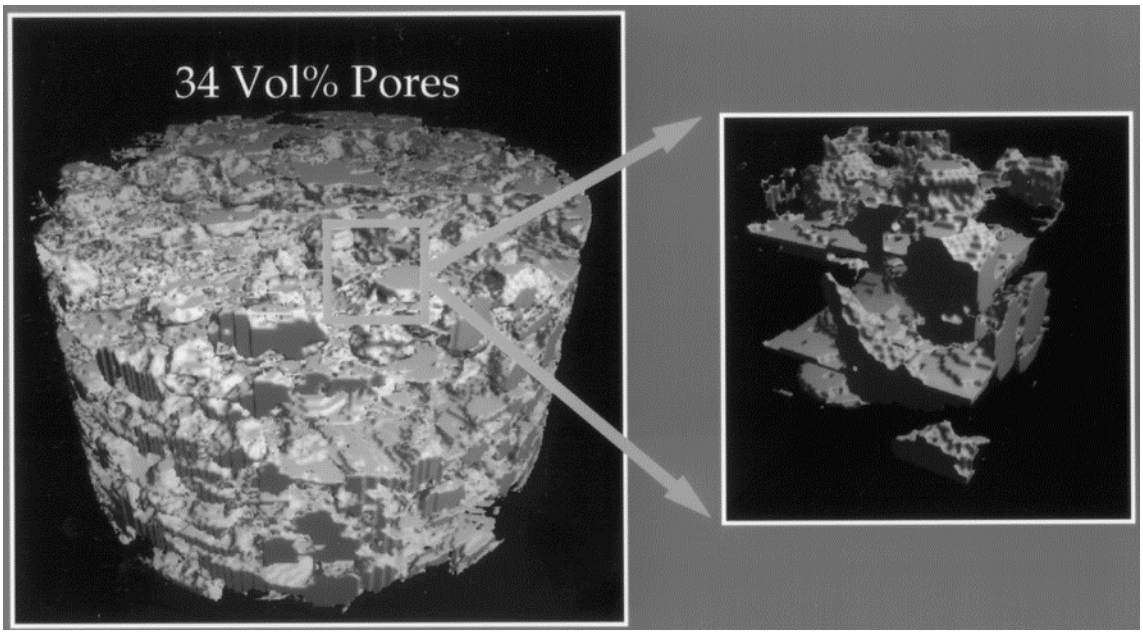

Fig. 8 X-tomograph of synthesized porous HAp showing the interconnected structure.

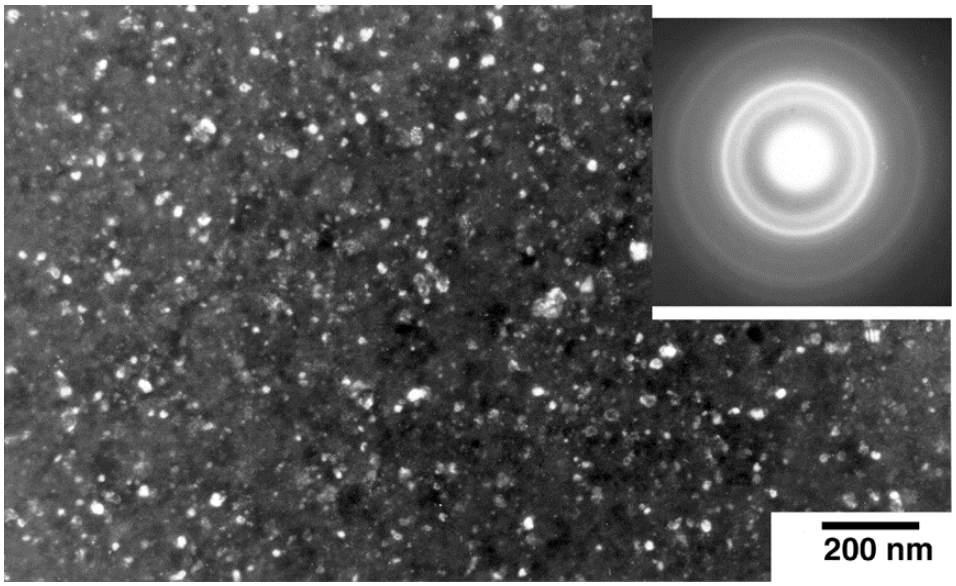

Fig. 9 TEM microstructure of a magnetron sputtered HAp film (0.65 μm) on a Ti/Si substrate.

The elastic modulus and hardness as a function of indentation depth of the 0.65-μm HAp coatings on Ti/Si and Si substrates are shown in Figs. 10a and 10b, respectively. The indentation measurements were terminated at a depth of 220 nm, which is about a third of the total HAp coating thickness. The initial drop in both modulus and hardness was usually associated with an uncertainty in determining contact area of the indenter upon nanoindentation. It is readily observed in Fig. 10 that, after the initial drop, the modulus and hardness both increase gradually with increasing indentation depth. This increase is evidently caused by a substrate effect. (The elastic modulus and hardness of Si (111) are about 160 and 13 GPa respectively [22]. The elastic modulus of Ti is about 116 GPa.) Taking into account the substrate effect, the elastic modulus and hardness of the HAp coatings are estimated to be 120 and 7.8 GPa, respectively. It is also noted in Fig. 10 that the modulus and hardness of HAp

coatings on the Si substrate are stiffer and harder than the coatings on the Ti-Si substrate. This is a result of the fact that Si is stiffer and harder than Ti.

In comparison, the microhardness of the fully dense sample is about 483 MPa. It is also noted that the HAp coating is much harder than the bulk. The large difference may be attributed to the difference in grain size. The grain size of the HAp coating is only about 20 nm. To the first approximation, $H \propto (1/d)^{-1/2}$, where H is the hardness and d grain size, and using the hardness value of 483 MPa for the fully dense hydroxyapatite, a hardness value for the coating is estimated to be about 6.0 GPa, which is only slightly lower than the experimental values.

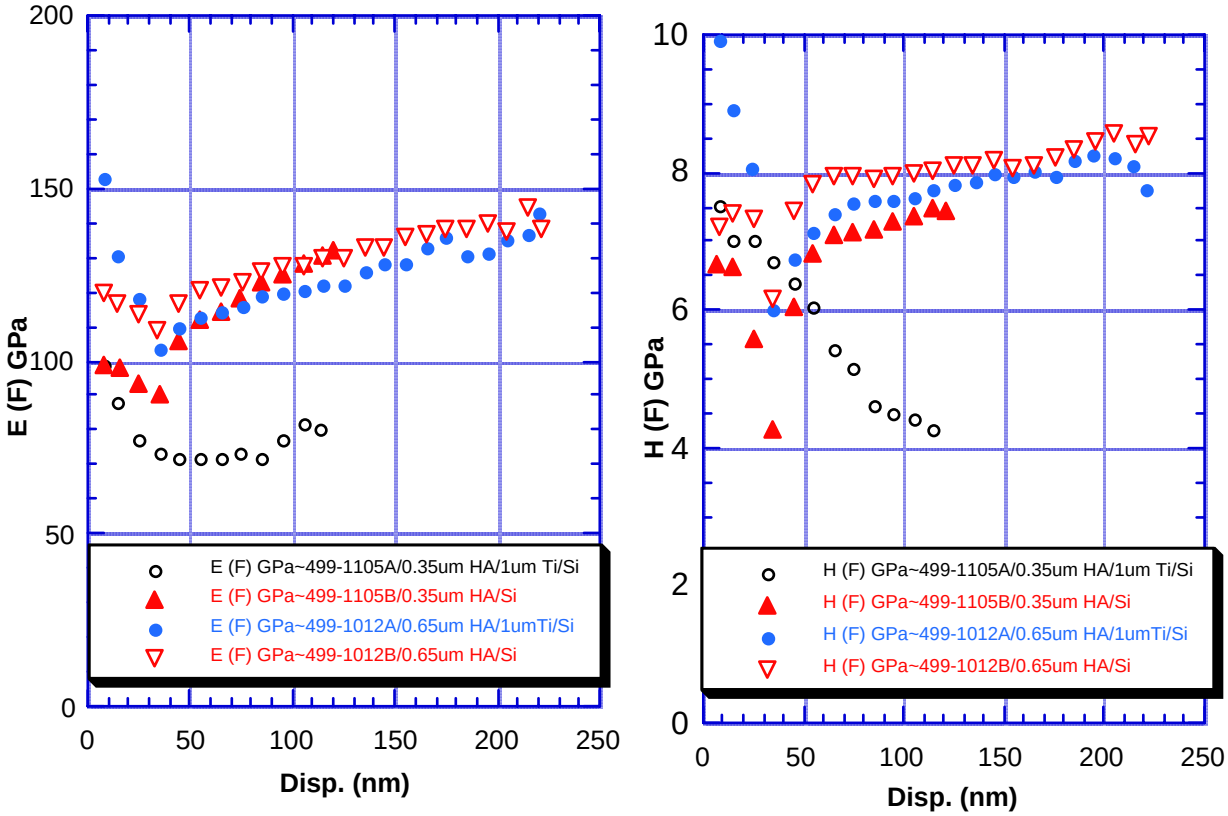

Fig. 10 Elastic modulus (a) and hardness (b) as a function of depth for several magnetron-sputtered hydroxyapatite films measured by nanoindentation techniques.

4. CONCLUSION

Hydroxyapatite (HAp) particles were produced by a chemical precipitation plus spray dry method. The sintering behavior of these HA nanocrystals was characterized. Both the density and microhardness of sintered samples increase with increasing temperature. The microhardness was found to be directly proportional to the density. Resulting from the fine HAp particles used in the present study, an accelerated sintering was observed. A relatively low activation energy for sintering was also obtained. Based on the kinetics, special efforts were made to synthesize cellular HAp structures. Porous structures with small cell (about 6 μm) were made. To synthesize porous structures with larger pores requires using larger starting HAp powder. To improve biocompatibility, experiments were also conducted to produce HAp coats Ti and Si substrates. Using nanoindentation techniques, the elastic modulus and hardness of the HAp coatings are estimated to be 120 and 7.8 GPa, respectively. The relatively high hardness value is a result of ultrafine grains in the coating. Further efforts are needed to

produce open-celled HAP structures with a pore size ~100-200 μm. Also, an evaluation of the HAp-Ti interfacial structure and interfacial strength are underway.

ACKNOWLEDGMENT

This work was performed under the auspices of the U.S. Department of Energy by LLNL under contract No. W–7405–Eng–48.

REFERENCES

1. L.L. Hench, *J. Am. Ceram. Soc.*, 81(7) (1998) 1705.
2. J.T. Tiffit, in *Fundamental and Clinical Bone Physiology*, *Chapter 3*, edited by M.R. Urist, Lippincott, Philadelphia, 1980.
3. M.D. Miller, *Review of Orthopaedics*, 2nd 2nd, W.B. Saunders Company, New York, 1992.
4. J.B. Park and R.S. Lakes, *Biomaterials*, 2nd 2nd, Plenum Press, New York, 1992.
5. A. Slosarczyk, *Powder Metall. Inter.*, 21(4) (1989) 24.
6. E.C. Shors and R.E. Holmes, in *An Introdcution to Bioceramics*, p. 181, edited by L.L. Hench and J. Wilson, World Scientific, Singapore, 1993.
7. M.B. Habal and A.H.R. Reddi, *Bone Grafts and Bone Substitutes*, 2nd 2nd, W.B. Saunders Company, New York, 1992.
8. T. Goto, N. Wakamatsu, H. Kamemizu, M. Iijima, Y. Doi, and Y. Moriwaki, *J. Mater. Sci. - Medicine*, 2 (1991) 149.
9. P. Van Landuyt, F. Li, J.P. Keustermans, J.M. Streydio, F. Delannay, and E. Munting, *J. Mater. Sci. - Medicine*, 6 (1995) 8.
10. P.E. Wang and T.K. Chaki, *J. Mater. Sci. - Medicine*, 4 (1993) 150.
11. G. de With, H.J.A. Van Dijk, N. Hattu, and K. Prijs, *J. Mater. Sci.*, 16 (1981) 1592.
12. K.A. Khor, Z.L. Dong, C.H. Quek, and P. Cheang, *Matet. Sci. Eng.*, A281 (2000) 221.
13. J.G.C. Wolke, K. van Dijk, H.G. Schaeken, K. de Groot, and J.A. Jansen, *J. Biomed. Mater. Res.*, 28(12) (1994) 1477.
14. K. Yamashita, T. Yagi, and T. Umegaki, *J. Am. Ceram. Soc.*, 79(12) (1996) 3313.
15. M. Yoshinari, Y. Ohtsuka, and T. Derand, *Biomater.*, 15(7) (1994) 529.
16. P. Luo and T.G. Nieh, *Biomater.*, 17(20) (1996) 1959.
17. W.D. Kingery, H.K. Bowen, and D.R. Uhlmann, *Introduction to Ceramics*, 2nd 2nd, John Wiley & Sons, Inc., New York, 1976.
18. M. Jarco, C.H. Bolen, M.B. Thomas, J. Bobick, J.F. Kay, and R.H. Doremus, *J. Mater. Sci.*, 11 (1976) 2027.
19. T. Kijima and M. Tsutsumi, *J. Amer. Ceram. Soc.*, 62 (1979) 455.
20. S.F. Hulbert and P.E. Young, *Use of Ceramics for Surgical Implants*, Gordon and Breach Science Publishers, New York. USA, 1978.
21. T.G. Nieh, J. Kinney, A.J.C. Ladd, and J. Wadsworth, *Scr. Mater.*, 38(10) (1998) 1487.
22. T.C. Chou, T.G. Nieh, S.D. McAdams, and G.M. Pharr, *Scr. Metall. Maters.*, 25 (1991) 2203.